Building and Environment 44 (2009) 2319–2326

Contents lists available at ScienceDirect

Building and Environment

journal homepage: www.elsevier.com/locate/buildenv

Simulation and testing of pollutant dispersion during preventive maintenance in a cleanroom

Hui-Ya Shih [a], Shih-Hsuan Huang [b], Shou-Nan Li [a], Sheng-Chieh Chen [b], Chuen-Jinn Tsai [b,*]

[a] Energy and Environment Research Laboratories, Industrial Technology Research Institute (ITRI), Hsin Chu, Taiwan
[b] Institute of Environmental Engineering, National Chiao Tung University, No. 75 Poai Street, Hsin Chu 300, Taiwan

ARTICLE INFO

Article history:
Received 16 December 2008
Received in revised form
2 March 2009
Accepted 18 March 2009

Keywords:
Airborne molecular contamination
Gas sensors
Cleanroom
Preventive maintenance

ABSTRACT

Sulfur hexafluoride (SF_6) of >99.9% purity was artificially released to simulate the emission sources in the etching-thin film area of a working cleanroom in a semiconductor fab at the rate of 492 g/h. Three mobile Fourier transform infrared spectrometers (FTIRs, detection limit: 10 ppb) were used simultaneously to measure the real time SF_6 concentrations at different locations of the cleanroom. A three-dimensional numerical model was also used to predict the unsteady gas concentration distribution and the results were compared with the experimental data. Due to high dilution of the pollutant in the cleanroom, it is found that the current gas sensors may not be sensitive enough and a better monitoring system and strategy is needed to protect workers from injury and to ensure good product yield. After comparison with the validated numerical results, the well-mixed model is found to predict the peak pollutant concentrations within a reasonable range which is 0.34–1.33 times the experimental values except when the monitored distance is very close to the release point. The well-mixed model is shown to be capable of predicting a reasonable attainable maximum concentration once a pollutant leaks in the cleanroom.

1. Introduction

Airborne contaminants pose a serious threat to the state-of-the-art manufacturing processes as the feature size continues to shrink in the semiconductor industry. When a gas pollutant leaks from the pipes, fittings or process chambers, it mixes with the recirculation air and disperses in the cleanroom to become an AMC (airborne molecular contamination), which will cause process tool damage, product corrosion, wafer defects and potential worker injury [1].

Many micro-contamination studies in the cleanroom have been conducted in the past. When the concentration of hydrogen chloride was higher than 28 ppb, the corrosion defects were observed on the test wafer [2]. The concentration of ammonia of 20 ppb could cause the critical dimension shift of 25–35% depending on the type of photo-resists [3]. When chemically amplified resist was left in an uncontrolled atmosphere of about 10 ppb NH_3, patterns on the wafers were either not developed or T-top phenomenon occurred [4]. Hazy optical lens was found in a TFT-LCD fab due to the continuous emission of high concentration of NH_3 into the cleanroom during the preventive maintenance (PM) process of the photo-resist stripper [5]. Ruthenium (Ru) airborne contaminant, which diffused to the cleanroom during cleaning of Ru CVD furnace tubes, was determined as a harmful gas to the MOSFETs process [6]. High concentrations of corrosive and toxic gases were found to emit from the metal etch chambers and downstream pipelines during PM process [7,8]. Without appropriate control, hydrogen chloride (HCl) as high as 343 ppm was detected inside the enclosed chamber, which might cause corrosion on the wafers and the process tools after the chamber was opened. Therefore, to ensure high yield manufacturing in the semiconductor industry, the pollutant concentration must be controlled below a certain limit. For example, the yield enhancement committee of the International Technology Roadmap for Semiconductors (ITRS) recommended that the concentration of the total inorganic acids and bases be less than 0.5 and 2.5 ppb, respectively, for reticle exposure environment, or less than 5.0 and 50.0 ppb, respectively, for lithography cleanroom environment for the years 2007–2015 [9]. To meet this stringent requirement, chemical filters are often used to reduce the AMC concentration in the cleanroom [2–4]. Mini-environment and SMIF (standard mechanical interface) enclosure are also useful tools to achieve the requirement of cleanliness [10]. The air-pressure differentials between mini-environment space and its surrounding space were found to be very low and yet were effective in maintaining low particle-concentration levels [11].

* Corresponding author. Tel.: +886 3 573 1880; fax: +886 3 572 7835.
E-mail address: cjtsai@mail.nctu.edu.tw (C.-J. Tsai).

0360-1323/$ – see front matter © 2009 Elsevier Ltd. All rights reserved.
doi:10.1016/j.buildenv.2009.03.018

Nomenclature

C	Courant number
C_{max}	maximum SF_6 concentration
C_μ, $C_{\varepsilon 1}$, $C_{\varepsilon 2}$	turbulence constants
F	diffusion flux component
I	turbulent intensity
k	turbulent kinetic energy (m^2/s^2)
l	turbulent mixing length (m)
ℓ	characteristic dimension (m)
m	mass fraction of the species (%)
p	static pressure (N/m^2)
U	inlet velocity (m/s)
u	fluid velocity(m/s)
u_n	superficial velocity normal to the surface of porous media
$\lvert\vec{V}\rvert$	characteristic velocity (m/s)
x, y, z	Cartesian coordinates (m)
α	inertia parameter
β	viscosity parameter
ΔP	airflow resistances (N/m^2)
Δt	iteration time step (s)
ε	turbulence energy dissipation rate (m^2/s^3)
μ	dynamic viscosity (Ns/m^2)
μ_t	turbulent dynamic viscosity (Ns/m^2)
μ_{eff}	$\mu + \mu_t$ (Ns/m^2)
ρ	density (kg/m^3)
σ_k, σ_ε	turbulence constants
τ_{ij}	stress tensor components (N/m^2)

Subscripts

i, j, k	index of Cartesian components
s	species

In addition, an effective ventilation control during preventive maintenance is an important method to reduce AMC contamination in the cleanroom [8].

However, AMC concentration in the cleanroom is non-uniform and unsteady, which requires an in-depth study. Chen et al. [12] studied the detailed flow and transient concentration fields of a gaseous pollutants emitted from a valve manifold box experimentally and numerically. Hot spots of the pollutant, the peak concentration and the time taken for reducing the pollutant concentration to the background level were found. Mora et al. [13] investigated two approaches for simulating the flow field in large indoor spaces. They suggested that coarse-grid k–ε CFD (Star-CD code) is more accurate than the zonal method, which was developed to provide an improvement over the well-mixed assumption for predicting airflows and contaminant transport. Zhang and Chen [14] used the inverse CFD model with the quasi-reversibility (QR) equation and numerical scheme to identify the gaseous contaminant sources in an aircraft cabin and an office. Choi and Edwards [15] conducted large eddy simulations to quantify contaminant transport due to the wakes generated by human motions. Sørensen et al. [16] recommended the following points to improve the quality of CFD: (1) the boundary/initial conditions and turbulence model should be detailed enough; (2) topology and size of the computational grid should be described; (3) influence from grid-dependency should be addressed; (4) use of differencing scheme should be described; (5) the range of the dimensionless distance from the wall should be stated and justified in accordance with the employed turbulence model; (6) the calculations should be validated against measurements or standard test cases of a similar problem.

This study used the similar experimental and numerical methods of Chen et al. [12] to investigate the spatial and temporal dispersion patterns of the gaseous pollutants in a working cleanroom during simulated preventive maintenance. The suitability of gas sensors and the applicability of the well-mixed model for predicting the pollutant concentration were then discussed in light of the dilution factors found in this study.

2. Experimental method

The experimental study was conducted in an ISO class 1, fan-filter-unit (FFU) type working cleanroom in one of the DRAM semiconductor fabs in Hsin Chu, Taiwan. Fig. 1a and b show the 2-D and 3-D schematic diagrams of the cleanroom, in which the 3rd, 4th and 5th floor of the plant are sub-fab layer, fab layer and supply air plenum, respectively. A total of 1900 FFUs located at the ceiling of the fab layer are used in the cleanroom. The FFUs of different working and maintenance zones are controlled at different rotation speeds by many different control panels. The FFUs were grouped into 65 regions and the air velocities at 0.3 m below the FFUs were measured by a TSI Model 8330 anemometer (TSI Inc., St. Paul, MN, USA) at 10 different points in each region. The flow rate of the make-up air is 168,448 CMH (m^3/h), or 4.7 air exchanges per hour. The pressure at each area and pressure difference between different areas are measured by sensors set up near the ceiling in the fab. The pressure and pressure difference are adjusted by the MAU and FFU systems.

For reference only, there are other new types of FFU systems and characterization methods. For example, an FFU system capable of controlling the air volumetric flow rate through a feedback control system was developed and found to supply uniform airflow distribution at the exit of the FFUs [17]. Functionality and dynamic energy performance of individual FFUs under applicable operation and control schemes were characterized by the laboratory characterization method and procedure [18]. The energy performance of five different mini-environments housed in a traditional cleanroom was quantified, and the magnitudes of energy-saving potential of the various design, operation, and management of clean spaces were evaluated [19].

Fig. 2 shows the layout of the fab layer, in which the static pressure is 1.1, 1.1, 1.2 and 1.8 mmH_2O in the etching, the thin film, the furnace and the lithography areas, respectively. The static pressure of the lithography area is higher than other areas and is expected to be cleaner. Since the lithography area has the cleanest requirement in the fab, the possibility of cross-contamination to the lithography area from the etching-thin film area was investigated in this study. The main source of the AMCs in the cleanroom is preventive maintenance, so this study was simulated experimentally. Additional numerical simulation of the gas pollutant dispersion was performed and the simulated pollutant concentrations were compared with the experimental data.

A simulated contamination source was set up in the maintenance zone between D and E working zones in the etching-thin film area of the fab layer, as shown in Fig. 3. Sulfur hexafluoride (SF_6) was used as the tracer gas, because it is inactive and harmless to human health and the wafer manufacture process, and does not decompose in the air [20]. The detection of FTIR is sensitive to SF_6 with the detection limit of $<$10 ppb.

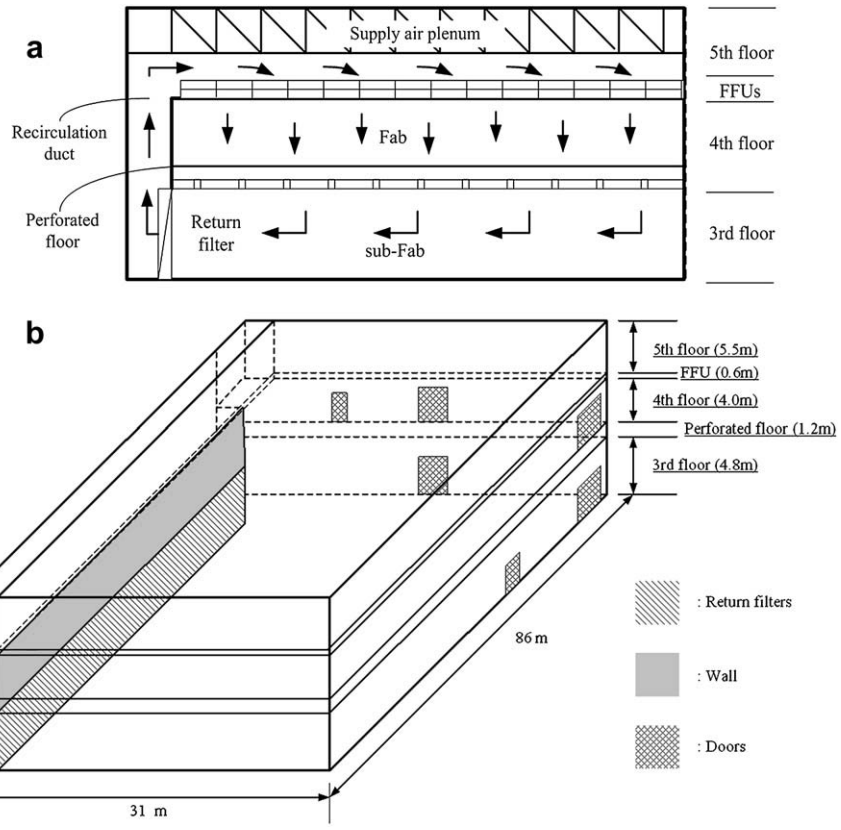

Fig. 1. (a) 2-D schematic diagram and air flow pattern in the FFU type cleanroom; (b) 3-D schematic diagram of the locations of the outlets.

The flow rate of the SF_6 gas (>99.9% in purity, Air Products San Fu Co. Ltd., Taiwan), 1.35 L/min, was controlled by a mass flow controller (Model No. 5850E, Brooks Instrument, USA) and released from 24 evenly distributed holes (ID = 2 mm) on a circular 1/4-inch Teflon tube placed at the bottom of the model chamber. Only when the total SF_6 mass emission rate was great than 492 g/h, which is the current emission rate, was the SF_6 concentration found to exceed the detection limit of the FTIR at every location in the cleanroom. The gas discharged from the Teflon tube was passed through a screen near the top of the chamber to improve the flow uniformity, as shown in Fig. 4. SF_6 gas was released for 10 min continuously then stopped.

Three mobile FTIRs (Work IR-104, ABB Bomem, Quebec, Canada) with a detection limit of 10 ppb were used simultaneously at three different locations to quantify the SF_6 concentration in the etching-thin-film areas for 10 min during 10-min SF_6 release and another 40 min after SF_6 release stopped. The monitoring points were located 1 m above the perforated floor and SF_6 concentrations were

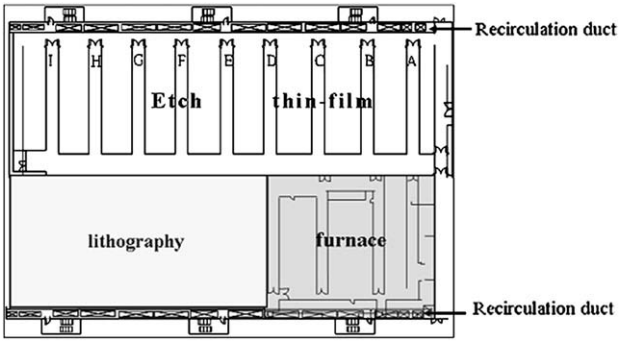

	W(width) × H(height) × L(length)		
Etching area	32m	16m	35m
Thin-film area	32m	16m	35m
Furnace	32m	16m	30m
Lithography	32m	16m	40m

Fig. 2. Layout and dimension of different working zones of the fab layer.

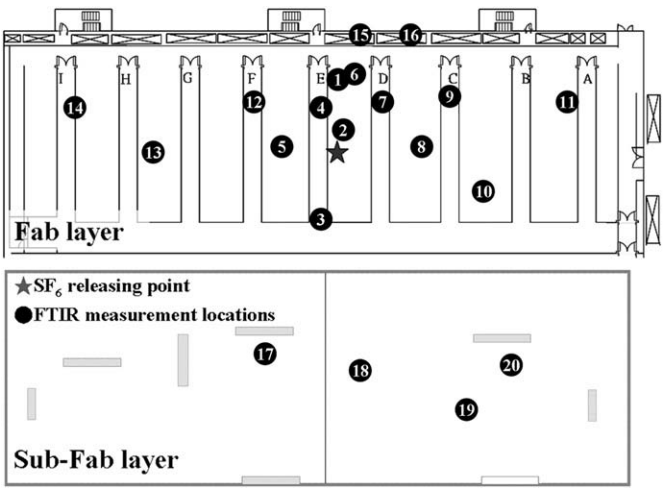

Fig. 3. Locations of the SF_6 source and the measurement points in the etching-thin film area.

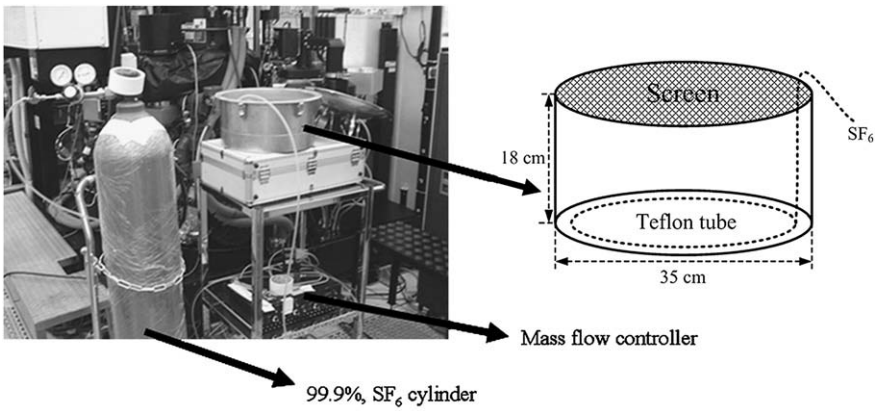

Fig. 4. Simulated SF_6 pollutant source from a model chamber.

recorded every 8 s by the three FTIRs. There were 20 measurement points (Nos. 1–20); 16 of these were on the fab layer and the other 4 on the sub-fab layer, as shown in Fig. 3. The selection of monitoring locations was based on the proximity of the releasing source as well as the consideration of full coverage of the cleanroom. After one single experiment, the three FTIRs were moved to different measurement points and the experiments were repeated until all 20 points were measured.

3. Numerical method

In the numerical study, the mass and momentum conservation equations were solved by the commercial software, STAR-CD (version 3.24, CD-Adapco Japan Co. Ltd). Assuming that the flow is steady and incompressible, the mass and momentum conservation equations are [21]:

$$\frac{\partial}{\partial x_j}(\rho u_j) = 0 \tag{1}$$

and

$$\frac{\partial}{\partial x_j}(\rho u_j u_i - \tau_{ij}) = -\frac{\partial p}{\partial x_i} \tag{2}$$

where x is the coordinate (m), subscripts i and j are the index of Cartesian components, u is the fluid velocity (m/s), ρ is the mass density (kg/m^3), τ_{ij} is the stress tensor (N/m^2), and p is the static pressure (Pa).

Standard k–εhigh Reynolds number model was used for simulating the turbulent flow in the cleanroom and the following two additional equations for k and ε were solved:

$$u_j\frac{\partial k}{\partial x_j} = \frac{1}{\rho}\frac{\partial}{\partial x_j}\left[\left(\mu + \frac{\mu_t}{\sigma_k}\right)\frac{\partial k}{\partial x_j}\right] + \frac{\mu_t}{\rho}\left(\frac{\partial u_i}{\partial x_j} + \frac{\partial u_j}{\partial x_i}\right)\left(\frac{\partial u_i}{\partial x_j}\right) - \varepsilon \tag{3}$$

and

$$u_j\frac{\partial \varepsilon}{\partial x_j} = \frac{1}{\rho}\frac{\partial}{\partial x_j}\left[\left(\mu + \frac{\mu_t}{\sigma_\varepsilon}\right)\frac{\partial \varepsilon}{\partial x_j}\right] + C_{\varepsilon 1}\frac{\varepsilon}{k}\frac{\mu_t}{\rho}\left(\frac{\partial u_i}{\partial x_j} + \frac{\partial u_j}{\partial x_i}\right)\left(\frac{\partial u_i}{\partial x_j}\right) - C_{\varepsilon 2}\frac{\varepsilon^2}{k} \tag{4}$$

where μ_t is the turbulent viscosity (Ns/m^2) defined as $\mu_t = C_\mu \rho k^2/\varepsilon$. The values assigned in the standard k–ε turbulence model coefficients, i.e. C_μ, $C_{\varepsilon 1}$, $C_{\varepsilon 2}$, σ_k and σ_ε, are 0.09, 1.44, 1.92, 1.0 and 1.22, respectively.

STAR-CD is based on the finite volume discretization method. The pressure–velocity linkage is solved by the SIMPLE (semi-implicit method for pressure linked equation) algorithm [22] and the differencing scheme for the space discretization method is the UD (upwind differencing) scheme. After the steady flow field was obtained, the unsteady SF_6 concentration field was calculated based on the mass conservation equation. The concentration of each constituent k in a fluid mixture, which is expressed as the mass fraction m_k, is governed by the following equation:

$$\frac{\partial}{\partial t}(\rho m_k) + \frac{\partial}{\partial x_j}\left(\rho u_j m_k - F_{k,j}\right) = 0 \tag{5}$$

where $F_{k,j}$ is its diffusion flux component of m_k.

Hexahedral cells were generated by an automatic mesh generation tool, Pro-Modeler 2003 (CD-Adapco Japan Co. Ltd). The total number of cells used is 2,740,736. The maximum length of the cell is about 50 cm and the minimum length is 1 cm near the releasing source of SF_6.

The convergence criterion of the flow field calculation was set to be 0.1% for the summation of the residuals. The total number of iterations to reach the flow field convergence is about 3000. For the transient calculation of the SF_6 concentration field, the time step is decided by the Courant number, C, which is calculated as:

$$C = \frac{|\vec{V}|\Delta t}{l} \tag{6}$$

where $|\vec{V}|$ and l are the characteristic velocity and dimension, respectively. In this study, the time step was set to be 0.1 s.

Flow velocity on the walls of the cleanroom was set to be zero at the boundaries. The uniform velocity boundaries at the inlets and outlets were assumed to be the average values of the velocities measured at the door openings. At the inlet boundaries, k and ε were given as $k = 1.5 \times (UI)^2$ and $\varepsilon = C_\mu^{0.75} \times k^{1.5}/\ell$, where U is the inlet velocity (m/s), I is the turbulent intensity, and ℓ is the turbulence length scale (m). In this study, ℓ was set to be 0.1. The exhaust flow rates drawn from the machine tools were set to be 60% and 40% at the outlet boundaries of the fab and sub-fab, respectively, according to the flow rates measured at the general ventilation ducts connecting to the exhausts of the tools.

The FFU cells in the model were treated as momentum sources based on the measured velocity data at 65 different regions as mentioned previously. The properties of the porous cells at four positions of the cleanroom were used to model the airflow resistance. The first position is the perforated floor, the second is the filters of FFUs, the third is the return filters and the fourth is the porous screen on the model process chamber. The airflow resistances ΔP in these units can be expressed as [21]:

Table 1
Air flow resistance parameter of porous cells.

	α_1	β_1	α_2	β_2	α_3	β_3
Perforated floor	1000	1000	1000	1000	50	50
FFU filter	1000	1000	1000	1000	30	30
Return filter	300	300	50	50	300	300
Porous screen of the model process chamber	1000	1000	1000	1000	42.92	9.7

$$\Delta P = \alpha_i u_n^2 + \beta_i u_n \quad (7)$$

where subscript $i = 1, 2, 3$ corresponds to x, y, z directions, respectively; α and β are parameters related to inertia and viscosity, respectively; u_n is the superficial velocity normal to the surface of porous media. α and β can be calculated based on Eq. (7) from the pressure drop versus flow velocity data measured in this study or provided by the manufacturer and the values are shown in Table 1.

4. Results and discussion

Experimental data of the gas concentration at the same locations were repeated and compared for precision. The comparison shows that the difference of the maximum peak concentration is less than 1.4% and the correlation coefficient of two repeated gas concentration distributions is higher than 0.91. It means that the present experiment has good precision. The simulated vertical velocities at 0.3 m below the FFUs are in good agreement with the measured data in 65 regions the FFUs. The maximum difference between the measured and simulated velocities is only 3.74%. In this cleanroom, air velocity averages about 0.27 m/s in the working zones and 0.55 m/s in the maintenance zones.

Fig. 5 shows the comparison of the experimental SF_6 concentrations with the simulated results at six different measurement points. Similar concentration distributions versus time can be seen with a maximum difference in the peak concentration between the measured and simulated values of <36%. The comparison at other locations is similar except at point 2 which is very close to the SF_6 release location (the distance is only 3.7 m). SF_6 was released from a model chamber for 10 min to simulate the PM process which caused the concentration to increase in the cleanroom. The maximum SF_6 concentration appears at about 1000 s (or 16.6 min) which is several minutes after SF_6 release stops, and then SF_6 continues to persist in the cleanroom for nearly another 40 min until its concentration drops to the background value.

The numerical result indicates that SF_6 gas is drifted downward quickly by the flow of the FFUs. After passing through the perforated floor, SF_6 flows rapidly near the top regions of the sub-fab to the recirculation duct and accumulates in the supply air plenum. The pollutant is then dispersed in the cleanroom quickly. Since the cleanroom air flow must go through the recirculation duct, which results in high pollutant concentration existing in the duct, the recirculation duct appears to be a good location to set up the gas sensors to detect the pollutant as quickly as possible.

4.1. Dilution factor of the cleanroom air

Based on this study, the characteristic of the pollutant dispersion at various locations of the cleanroom is discussed in light of the maximum attainable concentration and dispersion time. A summary of the experimental data at different measurement points in the cleanroom is listed in Table 2 during the 10-min SF_6 release at the rate of 492 g/h. In Table 2, C_{max} is the maximum SF_6

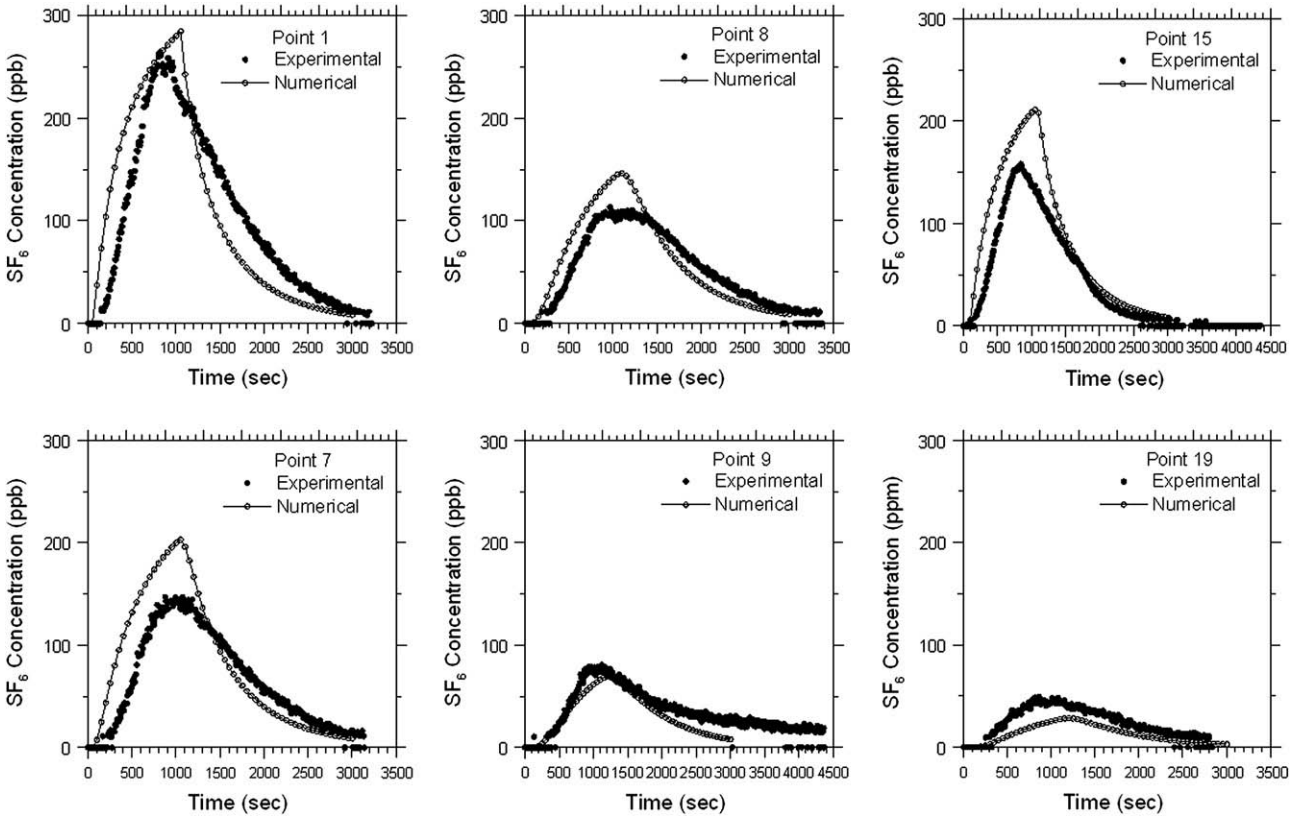

Fig. 5. Comparison of experimental SF_6 concentrations with simulated results at different locations.

Table 2
Characteristics of dispersed SF_6 concentration, emission rate: 492 g/h.

No.	C_{max} (ppb)	Dilution factor[a]	T_{max} (min)	$t_{10\%}$ (min)	Location
1	264	3.8E+06	13.6	29.7	fab
2	4939	2.0E+05	12.5	20.8	fab
3	114	8.8E+06	16.6	31.8	fab
4	238	4.2E+06	13.3	28.4	fab
5	86	1.2E+07	16.1	23.9	fab
6	231	4.3E+06	14.2	29.1	fab
7	147	6.8E+06	14.6	33.5	fab
8	113	8.8E+06	16.1	35.2	fab
9	81	1.2E+07	18.6	NA[b]	fab
10	104	9.6E+06	13	NA	fab
11	82	1.2E+07	16.3	NA	fab
12	86	1.2E+07	16.8	28.7	fab
13	68	1.5E+07	27.7	NA	fab
14	67	1.5E+07	27.7	NA	fab
15	158	6.3E+06	14.1	24	sub-fab
16	63	1.6E+07	32.7	NA	sub-fab
17	86	1.2E+07	20.1	30.5	sub-fab
18	654	1.5E+06	18.3	10.5	sub-fab
10	50	2.0E+07	14.4	NA	sub-fab
20	73	1.4E+07	18.6	NA	sub-fab
Ave.	385	9.7E+06	17.8	27.2	

[a] Average dilution factor is 9.2E+6 if point 2 is excluded.
[b] NA: when the concentration is lower than the detection limit of 10 ppb and T_{10} is not available.

Table 3
Gas sensors and default alarm setpoints (emission rate: 492 g/h).

Target gas	PEL (ppm)	Alarm setpoint of the sensor (ppm)	Conc. of process gas (%)	Max. conc. with 10^6 dilution (ppm)	If the alarm activates when the gas leaks?
AsH_3	0.05	0.05	1	0.01	No
BCl_3	5[a]	5	>99	0.99	No
BF_3	1[a]	3	>99	0.99	No
Cl_2	0.5	0.5	>99	0.99	Yes
ClF_3	0.1	0.3	>99	0.99	Yes
CO	35	25	>99	0.99	No
SiH_2Cl_2	5[a]	5	>99	0.99	No
F_2	1	1	1	0.01	No
HBr	3	3	>99	0.99	No
HCl	5	5	>99	0.99	No
HF	3	3	>99	0.99	No
CH_3OH	200	500	>99	0.99	No
NF_3	10	10	>99	0.99	No
NH_3	50	25	>99	0.99	No
PH_3	0.3	0.3	10	0.1	No
SiF_4	3[a]	3	>99	0.99	No
WF_6	3[a]	3	>99	0.99	No
SiH_4	5	5	>99	0.99	No
CH_4	15000	500	>99	0.99	No
H_2	12000	500	>99	0.99	No

[a] Ceiling limits.

concentration, T_{max} is the time for C_{max} to appear, and $t_{10\%}$ is the time required for SF_6 concentration to drop from its maximum value to 10% of the maximum value. The dilution factor is defined as the ratio of the released SF_6 concentration, or 100%, to C_{max}. As shown in the table, the maximum value of the C_{max} appears at point 2, 4939 ppb, since it is closest to the release point. The corresponding dilution factor is 2.0×10^5, while the minimum value of C_{max} (50 ppb) appears at point 20, and the corresponding dilution factor is 2.0×10^7. The dilution factor of the cleanroom air varies from 2.0×10^5 to 2.0×10^7. If point 2 is excluded, which is close to the releasing point, the range of the dilution factor is 1.0×10^6 to 2.0×10^7. The medium value of the above range is close to 5.0×10^6, which is calculated based on the maximum concentration predicted by the well-mixed model, 199.5 ppb, as will be shown in the next section.

In other words, when a gaseous pollutant is emitted into the cleanroom, the concentration of the pollution will be diluted to a large extent, which is about 10^5–10^7 if the emission time is 10 min and the emission rate is 492 g/h. Because of high dilution capacity of the cleanroom air, the toxic gas sensors in the cleanroom may not be able to set off the alarm for the concentration to exceed the permissible exposure limit (PEL). For example as shown in Table 3, when SiH_4 of 1000 ppm leaks from a pipe at 492 g/h for 10 min, the maximum SiH_4 concentration detected will be 1 ppb, which is much less than its PEL of 5 ppm. As many of the alarm limits are set at the PELs, most toxic gas sensors will never be activated unless the leak is very serious or very close to the gas sensors, or the PELs are low (e.g. Cl_2 and ClF_3).

Therefore a gas monitor with low detection limit is needed to protect the workers from injury. Similar or even lower detection limit of the gas monitors is needed to ensure a good product yield. These commercially available monitors include ion mobility spectroscopes (IMS), total molecular base real-time monitor (TMB-RTM), and some non-selective AMC monitors [23]. However, these monitors are expensive and cannot monitor multiple points at the same time, so a better monitoring strategy seems to be more desirable. One good monitoring strategy of AMCs is to monitor the recirculation air continuously as this study shows. The gas leak detection system (GLDS) comprising open-path FTIRs installed at the make-up air and recirculation air units was demonstrated to be a useful tool for locating the leaking spot from thousands of pipelines [1]. With the GLDs system, the fab engineers are able to efficiently reduce contamination emissions and avoid their adverse effects on wafer defects, facilities, products, and personnel.

Table 2 further shows that after the maximum SF_6 concentration is detected, it takes an average of 24.6 min ($t_{10\%}$ range: 10–30.5 min) for the concentration to drop to 10% of its maximum value. This result is useful for the emergency response center (ERC) to formulate an evacuation procedure in the interest of time.

It is to be noted that the above discussion is based on the dilution factor calculated using the present experimental condition. The dilution factor is subjected to change when the emission rate and the emission time of the pollutant are different, as will be discussed further in the next section.

4.2. Non-uniformity of gas pollutant distribution

The indoor air model was used to further characterize the dispersed pollutant concentration. Based on the mass conservation principle, the species concentration can be calculated as:

$$V\frac{dC_i}{dt} = kq_0C_o(1-F_0) + kq_1C_i(1-F_1) + kq_2C_o - k(q_0+q_1)C_i + S \quad (8)$$

where C is the concentration indoor (C_i) and outdoor (C_o); t is time; q is the volumetric flow rate for make-up air (q_0) and recirculation air (q_1), respectively; F is the filtration efficiency for make-up air (F_0) and recirculation air (F_1), respectively; V is the room volume; S is the indoor source emission rate; k is the factor characterizing the mixing condition ($k = 1$ for well-mixed condition). Based on Eq. (8) and assuming well-mixed conditions, the maximum concentration was calculated to be 199.5 ppb. This well-mixed value was used to calculate the non-uniformity factor, which is defined as the ratio of the measured maximum concentration to 199.5 ppb. The calculated non-uniformity factor in Table 4 shows that the factor decreases with an increasing distance from the sampling point to the SF_6 releasing source, and it ranges from 0.34 to 1.33 except at point 2, which is very close to the releasing source. That is, the well-mixed

Table 4
The non-uniformity factor in the etching-thin film area.

Scenario	No.	C_{max} (ppb)	Non-uniformity factor	Direct distance from source (m)
A	1	264	1.33	10.6
	2	4939	24.76	3.7
	3	114	0.57	10.9
	4	238	1.19	9.1
	5	86	0.43	6.7
	6	231	1.16	10.6
	7	147	0.74	8.9
	8	113	0.57	10.1
	9	81	0.4	15.2
	10	104	0.52	19.3
	11	82	0.41	29.3
	12	86	0.43	12.6
	13	68	0.34	23.7
	14	67	0.34	36.2

model is able to predict an attainable maximum concentration value within a reasonable range once a pollutant leaks into the cleanroom.

Fig. 6 shows the SF_6 concentration calculated by the well-mixed model and the simulated value at point 1 at different air exchange rates. It is seen that the well-mixed model predicts the maximum SF_6 concentration within a reasonable range. The predicted peak concentrations of 199.5 and 160.2 ppb are similar to the simulated values of 284.4 and 170.3 ppb for the air exchange rate of 4.7 and 7.8 times/h, respectively. However, the time to reach the maximum concentration is much shorter (or T_{max} is too short) and the drop from the peak concentration is too abrupt (or $t_{10\%}$ is too short) for both exchange rates. Increasing the air exchange rate from 4.7 to 7.8 times/h reduces the peak concentration by about 30%. That is, increasing the air exchange rate when a gas leak occurs is an effective way to remove the pollutant in the cleanroom once a gas leak occurs. It is also important to equip the cleanroom with controllable operation for individual and groups of FFUs as well as the main recirculation fan, especially in the case of pollutant leak that would require careful and immediate response to adjust air change rates.

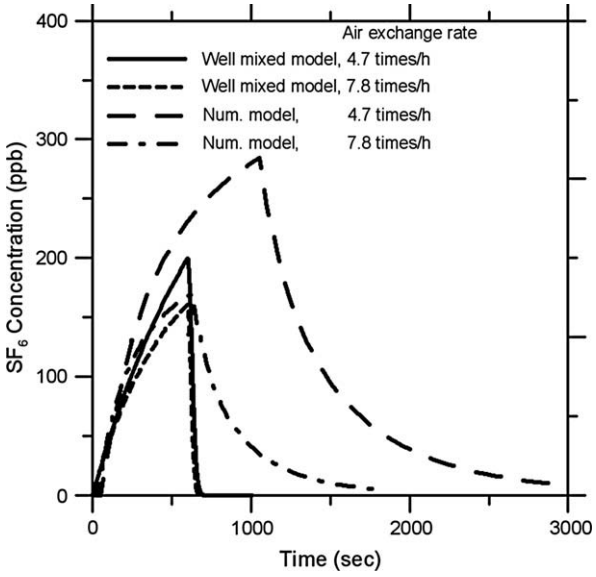

Fig. 6. Comparison of SF_6 concentration at different air exchange rates, point 1.

5. Conclusion

Experimental and numerical methods were used to investigate the spatial and temporal dispersion patterns of the gaseous pollutant in a working cleanroom during simulated preventive maintenance. Additional numerical simulation of the gas pollutant dispersion was performed and the simulated pollutant concentrations were compared with the experimental data. The numerical result indicates that SF_6 gas is drifted downward quickly by the flow of the FFUs. After passing through the perforated floor, SF_6 flows rapidly near the top regions of the sub-fab to the recirculation duct and accumulates in the supply air plenum. The pollutant is then dispersed in the cleanroom quickly. Since the cleanroom air flow must go through the recirculation duct, which results in high pollutant concentration existing in the duct, the recirculation duct appears to be a good location to set up the gas sensors to detect the pollutant as quickly as possible.

The toxic gas sensors in the cleanroom may not be able to set off the alarm for the high diluted concentration to exceed the permissible exposure limit (PEL). One good monitoring strategy of AMCs is to monitor the recirculation air continuously, as this study shows. The gas leak detection system (GLDS) consisting of open-path FTIRs at the make-up air and recirculation air units can be very useful for locating the leaking spot from thousands of pipelines. The well-mixed model is useful for estimating an attainable maximum concentration value once a pollutant leaks into the cleanroom. Increasing the air exchange rate when a gas leak occurs is an effective way to remove the pollutant in the cleanroom once a gas leak is detected. It is also important to equip the cleanroom with controllable operation for individual and groups of FFUs as well as the main recirculation fan, especially in the case of pollutant leak that would require careful and immediate response to adjust air change rates. With the dilution factor and non-uniformity factor, the fab engineers are able to estimate pollutant concentration quickly and take necessary action to avoid the adverse effects of pollutant on facilities, products, and personnel.

References

[1] Li SN, Leu GH, Yen SY, Chiou SF, Yu SJ, Hsu CF. Controlling contaminants with enhanced gas leak detection. Solid State Technology 2007;50(7):89–92.
[2] Higley JK, Joffe MA. Airborne molecular contamination: cleanroom control strategies. Solid State Technology 1996;39:211–2.
[3] Ruede D, Ercken M, Borgers T. The impact of airborne molecular base on DUV photoresists. Solid State Technology 2001;44:63–70.
[4] Kanzawa K, Kitano J. A semiconductor device manufacturer's efforts controlling and evaluating atmospheric pollution. IEEE/SEMI Advanced Semiconductor Manufacturing Conference; 1995. p.:190–193.
[5] Li SN, Shih HY, Shaw YY, Yang J. Case Study of Micro-Contamination Control. Aerosol and Air Quality Research 2007;7(3):432–42.
[6] Shimazaki A, Sakurai H, Nishiki K, Nadahara S. Controlling Ru airborne contamination in cleanroom. IEEE International semiconductor manufacturing symposium 2001:333–6.
[7] Li SN, Shih HY, Wang KS, Hsieh K, Chen YY, Chen YY, Chou J. Preventive maintenance measures for contamination control. Solid-State Technology 2005;48(12):53–6.
[8] Chien CL, Tsai CJ, Ku KW, Li SN. Ventilation control of air pollutant during preventive maintenance of a metal etcher in semiconductor industry. Aerosol and Air Quality Research 2007;7(4):469–88.
[9] International Technology Roadmap for Semiconductors (ITRS). Yield Enhancement; 2007, pp. 1–44. http://www.itrs.net/Links/2007ITRS/2007_Chapters/2007_Yield.pdf.
[10] Shiu HR, Huang HY, Chen SL, Ke MT. Numerical Simulation for air flow in the mini-Environment and SMIF enclosure. IEEE Transactions on Semiconductor Manufacturing 2003;16:60–7.
[11] Xu T. Characterization of minienvironments in a clean room: Design characteristics and environmental performance. Building and Environment 2007;42:2993–3000.
[12] Chen SC, Tsai CJ, Li SN, Shih HY. Dispersion of gas pollutant in a fan-filter-unit (FFU) cleanroom. Building and Environment 2007;42:1902–12.
[13] Mora L, Gadgil AJ, Wurtz E. Comparing zonal and CFD model predictions of isothermal indoor airflows to experimental data. Indoor Air 2003;13:77–85.

[14] Zhang TF, Chen Q. Identification of contaminant sources in enclosed environments by inverse CFD modeling. Indoor Air 2007;17:167–77.
[15] Choi JI, Edwards JR. Large eddy simulation and zonal modeling of human-induced contaminant transport. Indoor Air 2008;18:233–49.
[16] Sørensen DN, Nielsen PV. Quality control of computational fluid dynamics in indoor environments. Indoor Air 2003;13:2–17.
[17] Chen JJ, Lan CH, Jeng MS, Xu T. The development of fan filter unit with flow rate feedback control in a cleanroom. Building and Environment 2007;42:3556–61.
[18] Xu T. An innovative method for dynamic characterization of fan filter unit operation. Journal of the IEST 2007;50(2):85–97.
[19] Xu T. Characterization of minienvironments in a cleanroom: Assessing energy performance and its implications. Building and Environment 2008;43:1545–52.
[20] Heitbrink WA, Earnest GS, Mickelsen RL, Mead KR, D'arcy JB. Evaluation of leakage from a metal machining center using tracer gas methods: A case study. American Industrial Hygiene Association Journal 1999;60(6):785–8.
[21] Computational fluid dynamics software. STAR-CD version 3.24. Methodology. London: Computation Dynamic Limited; 2004.
[22] Patankar SV. Numerical heat transfer and fluid flow. Washington: Hemisphere Publishing Co; 1980.
[23] Robin Danfelt, Real-time monitors: Review and lithography applications. Semiconductor fabtech, 27th edition, pp. 100-106. http://www.fabtech.org.